Cubic-Spline Expansion with GA for Half-Space Inverse Problems

Wei Chien and Chien-Ching Chiu

Electrical Engineering Department, Tamkang University
Tamsui, Taiwan, R.O.C.
Email:chiu@ee.tku.edu.tw

Abstract — In this paper we address an inverse scattering problem whose aim is to determine the geometrical as well as the physical properties of a perfectly conducting cylindrical body buried in a half-space. We use cubic-spline method instead of trigonometric series to describe our shape and reformulated into an optimization problem and solved by the genetic algorithm. The genetic algorithm is employed to find out the global extreme solution of the object function. As a result, the shape of the scatterer, which is described by using cubic-spline, can be reconstructed. In such a case, fourier series expansion will fail. Even when the initial guess is far away from the exact one, the cubic-spline description and genetic algorithm can avoid the local extreme and converge to a global extreme solution. Numerical results are given to show that the shape description using cubic-spline method is much better than the Fourier series.

Index Terms — Inverse Problem, Cubic-spline, Fourier series.

I. INTRODUCTION

Due to large domain of applications such as non-destructive problem, geophysical prospecting and determination of underground tunnels and pipelines, etc., the inverse scattering problems related to the buried bodies has a particular importance in the scattering theory. In the past 20 years, many rigorous methods have been developed to solve the exact equations [1]-[9]. However, inverse problems of this type are difficult to solve because they are ill-posed and nonlinear [10]. As a result, many inverse problems are reformulated into optimization ones and then numerically solved by different iterative methods such as the Newton-Kantorovitch method [1]-[5], the Levenberg-Marquardt algorithm [6]-[8], and the successive-overrelaxation method [9]. Most of these approaches employ the gradient-based searching scheme to find the extreme of the cost function, which are highly dependent on the initial guess and usually get trapped in the local extreme. The genetic algorithm (GA) [11] is an evolutionary algorithm that uses the stochastic mechanism to search through the parameter space. As compared to the gradient-based searching techniques, the genetic algorithm is less prone to converge to a local extreme. This renders it an ideal candidate for global optimization. Recently, researchers have applied GA together with electromagnetic solver to attack the inverse scattering problem mainly in two ways. One is surface reconstruction approach; the other is volume reconstruction approach. Chiu [12] first applied the GA for the inversion of a perfectly conducing cylinder with the geometry described by a Fourier series (surface reconstruction approach), while Takenaka [13], Meng [14] and Zhou [15] used the concept of local shape function to describe the conducting objects (volume reconstruction approach). Alternatively, Chien [16], Zhou [17] and Qing [18] used b-splines to describe the geometry of a perfect conducting cylinder. The 2-d perfectly conducting cylinders are denoted by local shape functions $\rho = F(\theta)$ with respect to their local origins, which can be continuous or discrete. However, to the best of our knowledge, there are still no numerical results, which compared the cubic-spline and Fourier series, shape description with the genetic algorithm for the buried conducting scatterers. In this paper, we present a computational method based on the genetic algorithm to recover the shape of a buried cylinder. In Section II, a theoretical formulation for the inverse scattering is presented. The general principles of genetic algorithms and the way we applied them to the inverse problem are described. Numerical results for reconstructing objects of different shapes are given in Section III. Finally, some conclusions are drawn in Section IV.

II. THEORETICAL FORMULATION

Let us consider a perfectly conducting cylinder buried in a lossy homogeneous half-space, as shown in Fig 1. The media in regions 1 and 2 are characterized by the permittivity and conductivity $(\varepsilon_1, \sigma_1)$ and $(\varepsilon_2, \sigma_2)$, respectively, while the permeability μ_0 is used for each region, i.e., only non-magnetic media are concerned here. The cross-section of the cylinder is described by

polar coordinates in the xy plane through the shape function $\rho = F(\theta)$. The cylinder is illuminated by a plane wave with time dependence $\exp(j\omega t)$, of which the electric field is assumed parallel to the z-axis (i.e., transverse magnetic or TM polarization). Let E^{inc} denote the incident E-field from region 1 to region 2 with incident angle ϕ_1. Owing to the interface between region 1 and region 2, the incident plane wave would generate two waves in the absence of the conducting object: the reflected wave (for $y \le -a$) and the transmitted wave (for $y > -a$). Thus the unperturbed field is given by

$$\vec{E}_i(\vec{r}) = E_i(x,y)\hat{z} \tag{1}$$

with

$$E_i(x,y) = \begin{cases} E_1(x,y) = e^{-jk_1[x\sin\phi_1 + (y+a)\cos\phi_1]} \\ \qquad + R_1 e^{-jk_1[x\sin\phi_1 - (y+a)\cos\phi_1]}, y \le -a \\ E_2(x,y) = Te^{-jk_2[x\sin\phi_2 + (y+a)\cos\phi_2]}, y > -a \end{cases}$$

where

$$R_1 = \frac{1-n}{1+n}, T = \frac{2}{1+n}, n = \frac{\cos\phi_2}{\cos\phi_1}\sqrt{\frac{\varepsilon_2 - j\sigma_2/\omega}{\varepsilon_1 - j\sigma_1/\omega}}$$

$$k_1 \sin\phi_1 = k_2 \sin\phi_2$$

$$k_i^2 = \omega^2\varepsilon_i\mu_0 - j\omega\mu_0\sigma_i,\ i = 1,2 \quad \mathrm{Im}(k_i) \le 0 .$$

Note that each point can be expressed by (x, y) in Cartesian coordinates or (r, θ) in polar coordinates.

As the buried object is present, the scattered field can be expressed by

$$E_s(x,y) = -\int_0^{2\pi} G(x,y;F(\theta'),\theta')J(\theta')d\theta' \tag{2}$$

with

$$\vec{r} = (x,y), J(\theta) = -j\omega\mu_0\sqrt{F^2(\theta) + F'^2(\theta)}J_s(\theta)$$

$$G(x,y,x',y') = \begin{cases} G_1(x,y,x',y') & , y \le -a \\ G_2(x,y,x',y') = G_f(x,y,x',y') + G_s(x,y,x',y') & , y > -a \end{cases} \tag{3}$$

where

$$G_1(x,y,x',y') = \frac{1}{2\pi}\int_{-\infty}^{\infty} \frac{j}{\gamma_1 + \gamma_2} e^{j\gamma_1(y+a)} e^{-j\gamma_2(y'+a)} e^{-j\alpha(x-x')} d\alpha \tag{3a}$$

$$G_f(x,y,x',y') = \frac{j}{4} H_0^{(2)}[k_2\sqrt{(x-x')^2 + (y-y')^2}] \tag{3b}$$

$$G_s(x,y,x',y') = \frac{1}{2\pi}\int_{-\infty}^{\infty} \frac{j}{2\gamma_2}\left(\frac{\gamma_2 - \gamma_1}{\gamma_2 + \gamma_1}\right) e^{-j\gamma_2(y+2a+y')} e^{-j\alpha(x-x')} d\alpha \tag{3c}$$

$$\gamma_i^2 = k_i^2 - \alpha^2, i = 1,2, \mathrm{Im}(\gamma_i) \le 0, y' > a .$$

Here, $J_s(\theta)$ is the induced surface current density, which is proportional to the normal derivative of the electric field on the conductor surface. $G(x,y;x',y')$ is the Green's function which can be obtained by Fourier transform [3]. Note that we might face some difficulties in calculating the Green's function, since the Green's function given by (3) takes the form of an improper integral that must be evaluated numerically. However, the integral converges very slowly when (x, y) and (x', y') approach the interface, for which the acceleration of converging speed is possible by rewriting the Green's function as a closed-form term plus a rapidly converging integral (see Appendix). In (3b), $H_0^{(2)}$ is the Hankel function of the second kind of order zero. The boundary condition for a perfectly conducting object is

$$\hat{n} \times \vec{E} = 0 \tag{4}$$

where $\hat{n}$ is the outward unit vector normal to the surface of the scatterer. The boundary condition at the surface of the scatterer given by (4) leads to an integral equation for $J(\theta)$:

$$E_2(F(\theta),\theta) = \int_0^{2\pi} G_2(F(\theta),\theta;F(\theta'),\theta')J(\theta')d\theta' . \tag{5}$$

The total field E^{out} in region 1 is given by

$$E^{out}(r) = E_1(r) - \int_0^{2\pi} G_1(r;F(\theta'),\theta')J(\theta')d\theta' \ \ (y \le -a) . \tag{6}$$

The direct problem is to compute the total field in region 1 when the shape function $F(\theta)$ is given. This can be achieved by first solving for J from equation (5) and then calculating E^{out} by equation (6).

For numerical calculation of the direct problem, the contour is first divided into sufficient small segments so that the induced surface current can be considered constant over each segment. Then the moment method is used to solve equations (5) and (6) with a pulse basis function for current expansion and the Dirac delta function for testing [19].

Let us consider the following inverse problem, given the scattered electric field E_s measured outside the scatterer, and determine the shape $F(\theta)$ of the object.

(A) Using Fourier-series to describe the shape:

Assume the approximate center of the scatterer, which in fact can be any point inside the scatterer, is known. Then the shape function $F(\theta)$ can be expanded as:

$$F(\theta) \cong \sum_{n=0}^{\frac{N}{2}} B_n \cos(n\theta) + \sum_{n=1}^{\frac{N}{2}} C_n \sin(n\theta) \tag{7}$$

where B_n , and C_n , are real coefficients to be determined, and $N+1$ is the number of expanded terms.

(B) Using Cubic-spline to describe the shape:

The geometry of the cubic-spline is shown in Fig. 2. First, we separate the boundary of the shape with N pieces and we have $N+1$ separated points. We denote the separated points by polarized-coordinate

expression (ρ_0,θ_0) , (ρ_1,θ_1) ,..., (ρ_N,θ_N) , where $(0° \le \theta_i \le 360°)$, i=0…N, $\theta_0 = 0°$, $\theta_N = 360°$, and $\theta_0 < \theta_1 < ... < \theta_N$ ρ_i is the distance from point (ρ_i,θ_i) to the center point (x_0,y_0).

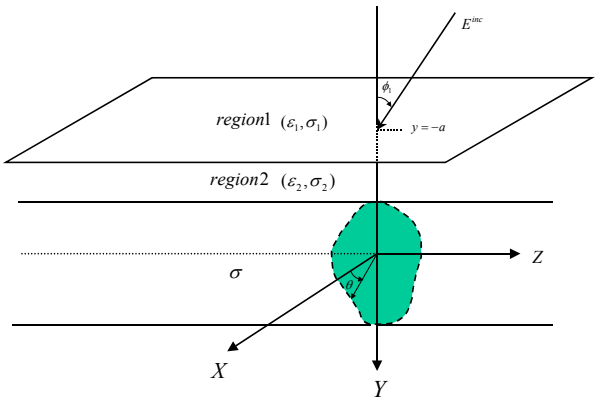

Fig. 1. Geometry of the problem in (x,y) plane.

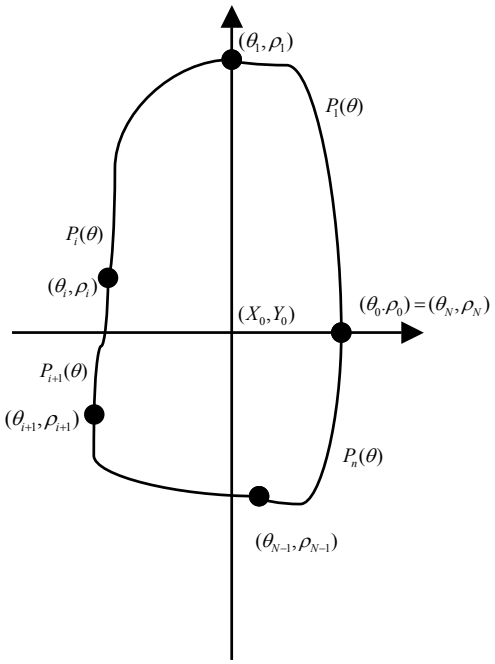

Fig. 2. Geometry of the cubic-spline.

Note that the discretization number of $J(\theta)$ for the inverse problem must be different from that for the direct problem. Since it is crucial that the synthetic data generated by a direct solver are not like those obtained by the inverse solver, the discretization number for the direct problem is twice of that for the inverse problem in this study. For the inversion procedure, the genetic algorithm is employed to maximize the following objective function:

$$SF = \left\{ \sum_{x=1}^{X_T} \left| E_s^{\exp}(\vec{r}_x) - E_s^{cal}(\vec{r}_x) \right|^2 \Big/ \sum_{x=1}^{X_T} \left| E_s^{\exp}(\vec{r}_x) \right|^2 + \beta \left| F'(\theta) \right|^2 \right\}^{-1/2} \tag{8}$$

where X_T is the total number of measured points. $E_s^{\exp}(\vec{r})$ and $E_s^{cal}(\vec{r})$ are the measured scattered field and the calculated scattered field, respectively. The minimization of $\beta|F'(\theta)|^2$ can, to a certain extent, be interpreted as the smoothness requirement for the boundary of $F(\theta)$. Therefore, the maximization of SF can be interpreted as the minimization of the least-square error between the measured and the calculated fields with the constraint of smooth boundary. Typical values of β range from 0.00001 to 10. The optimal value of β depends mostly on the dimensions of the geometry. One can always choose a large enough value to ensure the convergence, although overestimation would result in a very smooth reconstructed image. Technically, we can let the value of β decrease gradually during the course of convergence [4].

Genetic algorithms are the global optimization methods based on the genetic recombination and evolution in nature [11]. They use the iterative optimization procedures that start with a randomly generated population of potential solutions, and then gradually evolve toward a better solution through the application of the genetic operators. Genetic algorithms typically operate on a discretized and coded representation of the parameters rather than on the parameters themselves. These representations are considered as the "chromosomes", while the elements that constitute the chromosome are called "genes". Simple but often very effective chromosome representations for optimization problem involving several continuous parameters can be obtained through the juxtaposition of discretized binary representations of the individual parameters. In our problem, parameters B_n , C_n, and ρ_i are given by the following equation. As an example B_n is shown

$$B_n = p_{\min} + \frac{p_{\max} - p_{\min}}{2^L - 1} \sum_{i=0}^{L-1} b_i^{B_n} 2^i \tag{9}$$

where $b_0^{B_n}$, $b_1^{B_n}$, …and $b_{L-1}^{B_n}$ (gene) are the L-bit string of the binary representation of B_n , and P_{min} and P_{max} are the minimum and the maximum values admissible for B_n. Similar expressions exist for the parameters C_n and ρ_i and are omitted here for brevity. Here, P_{min} and P_{max} can be determined by prior knowledge of the object. Also, the finite resolution with B_n (C_n or ρ_i) can be tuned in practice by changing the number of bits

assigned to it. The basic GA for which a flowchart is shown in Fig. 3 starts with a large population containing a total of X candidates. Each candidate is described by a chromosome. Then, the initial population can simply be created by taking X random chromosomes. Then, the GA iteratively generates a new population that offspring from the previous population through the application of the reproduction, crossover, and mutation operators.

The new population contains increasingly better chromosomes and will eventually converge to a population that consists of the optimal chromosomes. As soon as the cost function (CF) changes by <1% in two successive generations or exceeds 1000 generations, the genetic algorithm will be terminated and the final solution is then obtained.

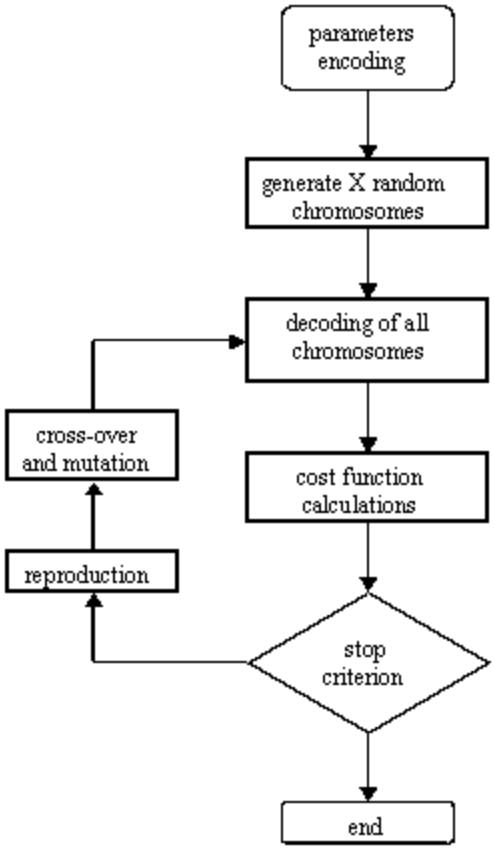

Fig. 3. The flowchart of GA.

III. NUMERICAL RESULT

Let us consider a perfectly conducting cylinder buried in a lossless half-space ($\sigma_1 = \sigma_2 = 0$). The permittivities in region 1 and region 2 are characterized by $\varepsilon_1 = \varepsilon_0$ and $\varepsilon_2 = 2.56\varepsilon_0$, respectively. A TM polarized plane wave of unit amplitude is incident from region 1 upon the object in region 2 as shown in Fig. 1. The frequency of the incident wave is chosen to be 3GHz, of which the wavelength λ_0 in free space is 0.1m. The object is buried at a depth $a \cong \lambda_0$ and the scattered fields are measured on a probing line along the interface between region 1 and region 2. Our purpose is using the Fourier-series and cubic-spline shape expressions to reconstruct the shape and comparing which is better in the inverse problem. The object is illuminated by three incident waves from different directions, while 20 measurement points at equal spacing are used along the interface $y = -a$ for each incident angle. There are 60 measurement points in each simulation. The measurement is taken from x=0 to 0.2m for incident angle $\phi_1 = -60°$, from x=-0.1 to 0.1m for incident angle $\phi_1 = 0°$, and from x=-0.2 to 0m for incident angle $\phi_1 = 60°$. To save computing time, the number of unknowns is set to be 7, and the population size is chosen as 300 (i.e. X =300). The binary string length of the unknown coefficient, B_n (C_n and ρ_l), is set to 20 bit (i.e., L=20). The search range for the unknown coefficient of the shape function is chosen to be from 0 to 0.1. The extreme values of the coefficients of the shape function can be determined by some priori knowledge of the objects. Here, the prior knowledge means that we can get the approximate position and the size of the buried cylinder by first using tomography technique, and then get the exact solution by the genetic algorithm. The crossover probability p_c and mutation probability p_m are set to be 0.8 and 0.1, respectively. The value of β in equation (6) is chosen to be 0.001.

In the first example, the shape function is given by $F(\theta) = (0.03 + 0.015\cos 3\theta)$ m and we use Fourier-series and cubic-spline expressions to recover it. The reconstructed shape function for the best population member (chromosome) is plotted in Fig. 4(a), respectively, with the error shown in Fig. 4(b). Here, DR, which is called shape function discrepancies, is defined as

$$DR = \{\frac{1}{N'}\sum_{i=1}^{N'}[F^{cal}(\theta_i) - F(\theta_i)]^2 / F^2(\theta_i)\}^{1/2} \qquad (10)$$

where N' is set to 60. The quantities DR provide measures of how well $F^{cal}(\theta)$ approximates $F(\theta)$. From Fig. 4, it is clear that reconstruction of the shape function is quite good for both Fourier-series and cubic-spline expressions. To investigate the sensitivity of the imaging algorithm against random noise, two independent Gaussian noises with zero mean have been added to the real and imaginary parts of the simulated scattered fields. Normalized standard deviations of 10^{-5} , 10^{-4} , 10^{-3} , 10^{-2} , and 10^{-1} are used in the

simulations. The normalized standard deviation mentioned earlier is defined as the standard deviation of the Gaussian noise divided by the rms value of the scattered fields. Here, the signal-to-noise ratio (SNR) is inversely proportional to the normalized standard deviation. The numerical result for this example is plotted in Fig. 4(b).

In the second example, we selected cubic-spline to describe the shape $\rho_1 = 0.02$ m, $\rho_2 = 0.02\sqrt{3}$ m, $\rho_3 = 0.02\sqrt{3}$ m, $\rho_4 = 0.02$ m, $\rho_5 = 0.02\sqrt{3}$ m, $\rho_6 = 0.02\sqrt{3}$ m. We can see that the 7-terms Fourier-series expression cannot recover the shape. The purpose of this example is to show that cubic-spline method is able to reconstruct a scatter while the Fourier-series fails. Both the shape results are shown in Fig. 5(a) and the relative error of Cubic-spline expand is shown in Fig. 5(b).

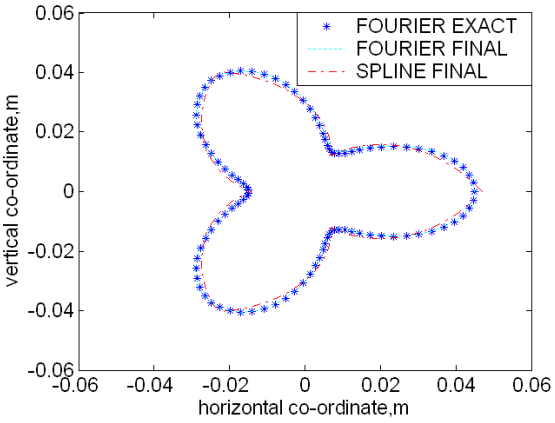

Fig. 4(a). Shape function for example 1. The star curve represents the exact shape by the Fourier-series, while the curve of short imaginary line is calculated shape by the Fourier-series and the curve of long imaginary line represents calculated shape by the cubic-spline in final result.

In the third example, the shape and conductivity function are selected to be $F(\theta) = (0.03 + 0.005\cos\theta + 0.005\cos 2\theta + 0.005\cos 3\theta)$ m. Note that the shape function is not symmetrical about either x-axis or y-axis. Both Fourier-series and cubic-spline expressions can recover it. Refer to Fig. 6(a) and Fig. 6(b) for details.

In the fourth example, we selected cubic-spline to describe the shape ρ_0 = 0.03 m, ρ_1 = 0.02 m, ρ_2 = 0.01 m, ρ_3 = 0.01 m, ρ_4 = 0.01 m, ρ_5 = 0.03 m, and slope is 5. Again 7-terms Fourier series expression cannot recover the shape. Both the shape results are shown in Fig. 7(a) and the relative error of Cubic-spline expand is shown in Fig. 7(b).

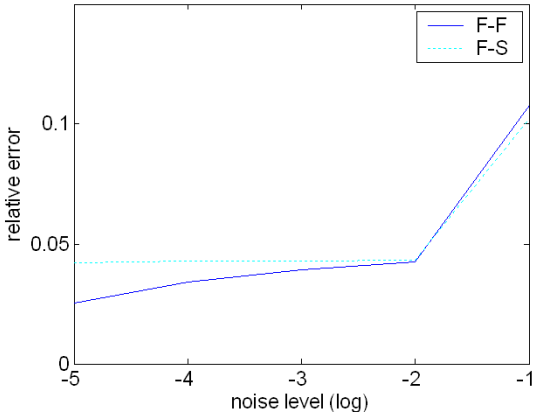

Fig. 4(b). Shape function error in each represented method. The F-F means that the shape functions both in direct and inverse problems are described by the Fourier-series. The F-S means that the shape function in the direct problem is described by the Fourier-series and in the inverse problem is described by the cubic-spline.

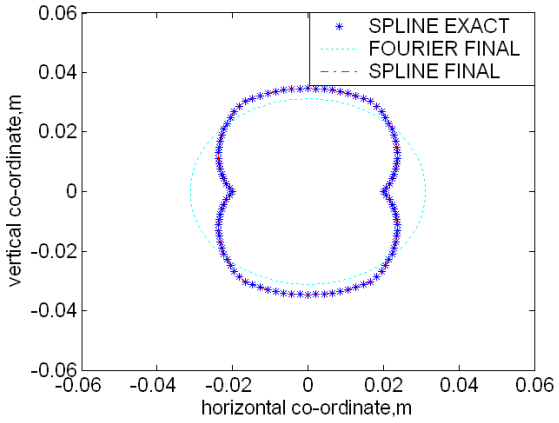

Fig. 5(a). Shape function for example 2. The star curve represents the exact shape by the Fourier-series, while the curve of short imaginary line is calculated shape by the Fourier-series and the curve of long imaginary line represents calculated shape by the cubic-spline in final result.

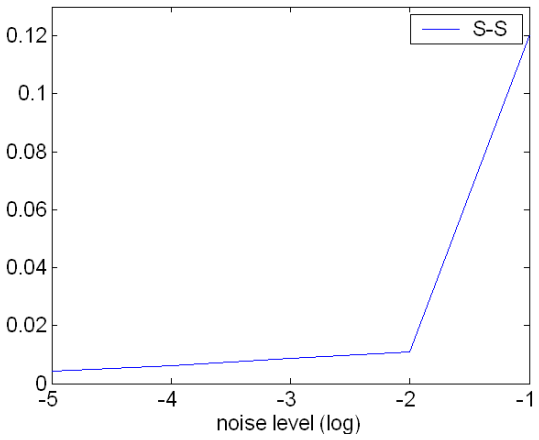

Fig. 5(b). Shape function error in each represented method. The S-S means that the shapefunctions both in the direct and inverse problem are described by the cubic-spline.

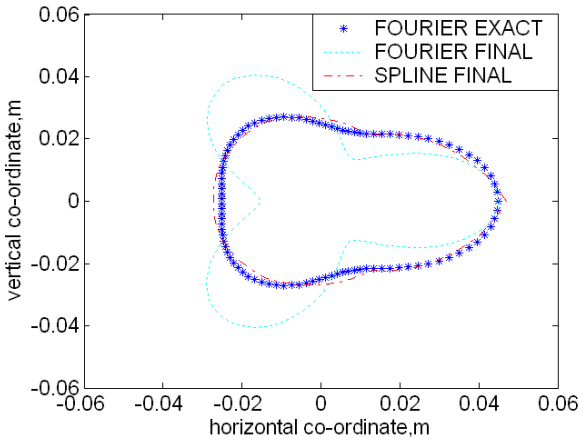

Fig. 6(a). Shape function for example 3. The star curve represents the exact shape by the cubic-spline, while the curve of short imaginary line is calculated shape by the Fourier-series and the curve of long imaginary line represents calculated shape by the cubic-spline in final result.

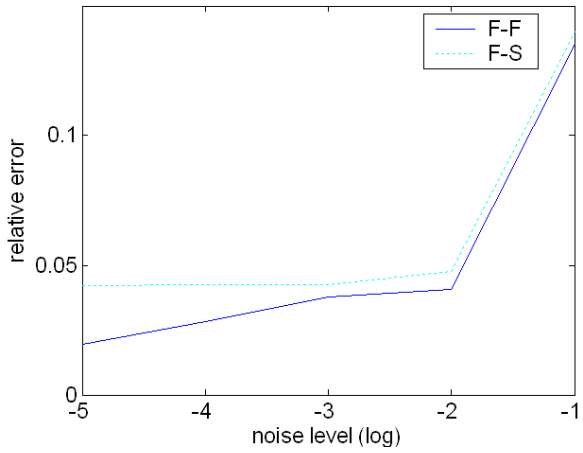

Fig. 6(b). Shape function error in each represented method. The F-F means that the shape functions both in the direct and inverse problems are described by the Fourier-series. The F-S means that the shape function in the direct problem is described by the Fourier-series and in the inverse problem is described by the cubic-spline.

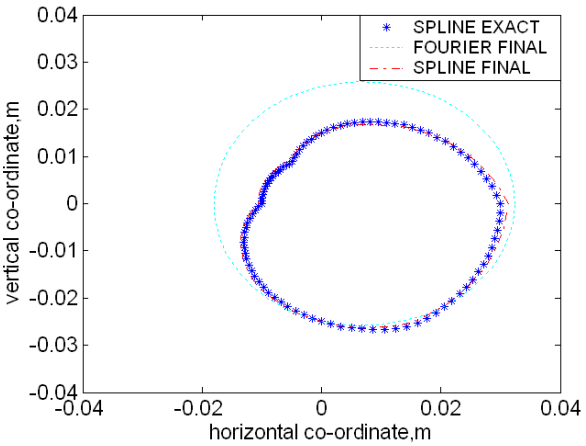

Fig. 7(a). Shape function for example 4. The star curve represents the Fourier-series exact shape, while the curve of short imaginary line is the Fourier-series calculated shape and the curve of long imaginary line is represents the cubic-spline calculated shape in final result.

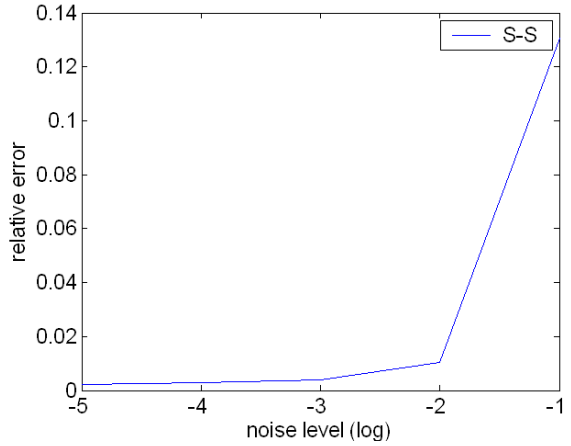

Fig. 7(b). Shape function error in each represented method. The S-S means that the shape functions both in the direct and inverse problems are described by the cubic-spline.

IV. CONCLUSION

We have presented a study of applying the genetic algorithm to reconstruct the shape of a buried metallic object through the measurements of scattered E fields. Based on the boundary condition and the measured scattered fields, we have derived a set of nonlinear integral equations and reformulated the imaging problem into an optimization one. The contours of the cylinders are denoted by cubic-spline local shape functions in local polar coordinate instead of trigonometric series local functions to guarantee the nonnegative definiteness. Experiment results show that the variable searching ability of GA has its limitation, and Fourier-series expression cannot recover the arbitrary shape in finite terms. In our numerical results, it is shown that using cubic-spline expand to describe the shape in the half-space inverse problem is more suitable than Fourier-series expression.

ACKNOWLEDGEMENT

This work was supported by National Science Council, Republic of China, under Grant NSC-91-2219-E-032-004.

Autobiography

Wei Chien was born in Taipei, Taiwan, Republic of China, on April 21, 1974. He received the B.S.E.E. degree from Tatung Institute of Technology, Taipei, Taiwan, in 1997 and M.S.E.E. degree from Tamkang University, Taipei, Taiwan, in 1999. From 1999 to 2001, he served in the ROC Army Force as a second lieutenant. He is working toward Ph.D degrees in the Department of Electrical Engineering, Tamkang University, now. His current research interests include numerical techniques in electromagnetics and wireless communications.

Chien-Ching Chiu was born in Taoyuan, Taiwan, Republic of China, on January 23, 1963. He received the B.S.C.E. degree from National Chiao Tung University, Hsinchu, Taiwan, in 1985 and M.S.E.E. and ph.D degrees from National Taiwan University, Taipei, Taiwan, in 1987 and 1991 respectively. From 1987 to1989, he served in the ROC Army Force as a communication officer. In 1992 he joined the faculty of the Department of Electrical Engineering, Tamkang University, where he is now a Professor. He was a visiting scholar at the MIT and University of Illinois, Urbana from 1998 to 1999. His current research interests include microwave imaging, numerical techniques in electromagnetics and indoors wireless communications.

APPENDIX

To calculate the Green's function, we can use the following formula,

$$\int_u^\infty x^{r-1}e^{-\beta x}\cos\delta x dx = \frac{1}{2}(\beta+j\alpha)^{-r}\Gamma[r,(\beta+j\delta)u]+\frac{1}{2}(\beta-j\alpha)^{-r}\Gamma[r,(\beta-j\delta)u]$$

for $\mathrm{Re}\,\beta > |\mathrm{Im}\,\delta|$ (A1)

where $\Gamma(\alpha,Z)=\int_z^\infty e^{-t}t^{\alpha-1}dt$

Γ is the incomplete Gamma function that satisfies

$$\Gamma(-n,z)=\frac{(-1)^n}{n!}\left[\Gamma(0,Z)-e^{-z}\sum_{m=0}^{n-1}(-1)^m\frac{m!}{z^{m+1}}\right]$$

$$\Gamma(0,z)=-\gamma-\ln z-\sum_{n=1}^{\infty}(-1)^n\frac{z^n}{(n+1)!}\qquad [|\arg(z)|<\pi]$$

(A2)

γ is Euler's constant, i.e., γ =0.5772156649. Let us consider the following integral

$$G_1=\frac{1}{2\pi}\int_{-\infty}^{\infty}\frac{j}{\gamma_1+\gamma_2}e^{j\gamma_1(y+a)}e^{-j\gamma_2(y'+a)}e^{-j\alpha(x-x')}d\alpha$$

$$=\frac{1}{\pi}\int_0^{\infty}\frac{j}{\gamma_1+\gamma_2}e^{j\gamma_1(y+a)}e^{-j\gamma_2(y'+a)}\cos\alpha\,(x-x')\,d\alpha$$

where $\gamma_i^2=k_i^2-\alpha^2, i=1,2,3$ $Im(\gamma_i)\le 0$, $y'>-a$.

The integral G_1 may be rewritten as follows

$$G_1=\frac{1}{\pi}\int_0^{\infty}\frac{j}{\gamma_1+\gamma_2}e^{j\gamma_1(y+a)}e^{-j\gamma_2(y'+a)}\cos\alpha(x-x')d\alpha$$

$$+\frac{1}{2\pi}\int_{\alpha_0}^{\infty}\frac{1}{\alpha}e^{-\alpha(y'-y)}\cos\alpha(x-x')d\alpha$$

$$-\frac{1}{2\pi}\int_{\alpha_0}^{\infty}\frac{1}{\alpha}e^{-\alpha(y'-y)}\cos\alpha(x-x')d\alpha$$

In general, we choose $\alpha_0 >> |k_i|$, $i = 1, 2$. From Eq. (A1), we get

$$-\frac{1}{2\pi}\int_{\alpha_0}^{\infty}\frac{1}{\alpha}e^{-\alpha(y'-y)}\cos\alpha(x-x')d\alpha$$
$$=-\frac{1}{4\pi}\left\{\Gamma\left[0,\left[(y-y')+j(x-x')\right]\alpha_0\right]+\Gamma\left[0,\left[(y-y')-j(x-x')\right]\alpha_0\right]\right\}.$$

Using the above relation, we obtain

$$G_1=\frac{1}{\pi}\int_0^{\infty}\frac{j}{\gamma_1+\gamma_2}e^{j\gamma_1(y+a)}e^{-j\gamma_2(y'+a)}\cos\alpha(x-x')d\alpha$$
$$+\frac{1}{2\pi}\int_{\alpha_0}^{\infty}\frac{1}{\alpha}e^{-\alpha(y'-y)}\cos\alpha(x-x')d\alpha$$
$$-\frac{1}{4\pi}\left\{\Gamma\left[0,\left[(y-y')+j(x-x')\right]\alpha_0\right]+\Gamma\left[0,\left[(y-y')-j(x-x')\right]\alpha_0\right]\right\}. \quad \text{(A3)}$$

Now, the integral G_1 is written as a rapidly converging integral plus a dominant integral, which can be easily calculated by means of Simpson's rule. Similarly, we have

$$G_s=\frac{1}{2\pi}\int_{-\infty}^{\infty}\frac{J}{2\gamma_2}\left(\frac{\gamma_1-\gamma_2}{\gamma_1+\gamma_2}\right)e^{-j\gamma_2(y+2a+y')}e^{-j\alpha(x-x')}d\alpha$$
$$=\begin{bmatrix}\frac{1}{\pi}\int_0^{\infty}\frac{j}{2\gamma_2}\left(\frac{\gamma_2-\gamma_1}{\gamma_2+\gamma_1}\right)e^{-j\gamma_2(y+2a+y')}\cos\alpha(x-x')d\alpha\\ -\frac{k_2^2-k_1^2}{8\pi}\int_{\alpha_0}^{\infty}\frac{1}{\alpha^3}e^{-\alpha(y+2a+y')}\cos\alpha(x-x')d\alpha\end{bmatrix}$$
$$+\frac{k_2^2-k_1^2}{16\pi}\begin{Bmatrix}\left[(y+2a+y')+j(x-x')\right]^2\Gamma\times\\ \left[-2,\left[(y+2a+y')+j(x-x')\right]\alpha_0\right]+\\ \left[(y+2a+y')-j(x-x')\right]^2\Gamma\times\\ \left[-2,\left[(y+2a+y')-j(x-x')\right]\alpha_0\right]\end{Bmatrix}.$$

References

[1] A. Roger, "Newton-Kantorovitch algorithm applied to an electromagnetic inverse problem," *IEEE Trans. Antennas Propagat*., vol. AP-29, pp. 232-238, Mar. 1981.

[2] C. C. Chiu and y. W. Kiang, "inverse scattering of a buried conducting cylinder,"*Inverse Problems*, vol. 7, pp. 187-202, April 1991.

[3] C. C. Chiu and y. W. Kiang, "microwave imaging of multiple conducting cylinders," *IEEE Trans. Antennas propagat*., vol. 40, pp. 933-941, Aug. 1992.

[4] G. P. Otto and W. C. Chew, "Microwave inverse scattering-local shape function imaging for improved resolution of strong scatterers." *IEEE Trans. Microwave Theory Tech*., vol. 42, pp. 137-142, Jan. 1994.

[5] Kress R. "A Newton method in inverse obstacle scattering Inverse Problem in Engineering Mechanics," ed H D Bui et al (Rotterdam: Balkema), pp. 425-432, 1994.

[6] D. Colton and P. Monk, "A novel method for solving the inverse scattering problem for time-harmonic acoustic waves in the resonance region II," *SIAM J. Appl. Math*., vol. 46, pp. 506-523, June 1986.

[7] A. Kirsch, R. Kress, P. Monk, and A. Zinn, "Two methods for solving the inverse acoustic scattering problem, " *Inverse Problems*, vol. 4, pp. 749-770, Aug. 1998.

[8] F. Hettlich, "Two methods for solving an inverse conductive scattering problem," *Inverse Problems*, vol. 10, pp. 375-385, 1994.

[9] R. E. Kleinman and P. M. Van Den Berg, "Two-dimensional location and shape reconstruction," *Radio Sci.*, vol. 29, pp. 1157-1169, July-Aug. 1994.

[10] T. Hohage, "Iterative methods in inverse obstacle scattering: regularization theory of linear and nonlinear exponentially ill-posed problems," Dissertation Linz, 1999.

[11] D. E. Goldgreg, Genetic Algorithm in Search, Optimization and Machine Learning, Addison-Wesley, 1989.

[12] C. C. Chiu and P. T. Liu, "Image reconstruction of a perfectly conducting cylinder by the genetic algorithm," *IEE Proc.-Micro. Antennas Propagat.*, vol. 143, pp. 249-253, June 1996.

[13] T. Takenaka and Z. Q. Meng, T. Tanaka, W. C. Chew "Local shape function combined with genetic algorithm applied to inverse scattering for strips", *Microwave and Optical Technology Letters,* vol. 16, pp. 337-341, Dec. 1997.

[14] Z. Q. Meng, T. Takenaka and T. Tanaka, "Image reconstruction of two-dimensional impenetrable objects using genetic algorithm", *Journal of Electromagnetic Waves and Applications,* vol. 13, pp. 95-118, 1999.

[15] Y. Zhou and H. Ling "Electromagnetic inversion of Ipswich objects with the use of the genetic algorithm", *Microwave and Optical Technology Letters,* vol. 33, pp. 457-459, June 2002.

[16] W. Chien, "Using the Genetic Algorithm to reconstruct the two-dimensional conductor" Master Thesis, National Tamkang University, Department of Electrical Engineering, June 1999.

[17] Y. Zhou, J. Li and H. Ling; "Shape inversion of metallic cavities using hybrid genetic algorithm combined with tabu list", *Electronics Letters,* vol. 39, pp. 280 -281, Feb. 2003.

[18] A. Qing "An experimental study on electromagnetic inverse scattering of a perfectly conducting cylinder by using the real-coded genetic algorithm", *Microwave and Optical Technology Letters,* vol. 30, pp. 315-320, Sept. 200.1

[19] F. M. Tesche, "On the inclusion of loss in time domain solutions of electromagnetic interaction problems," *IEEE Trans. Electromagn. Compat.*, vol. 32, pp. 1-4, 1990.

[20] E. C. Jordan and K. G. Balmain, Electromagnetic Waves and Radiating systems. Englewood Cliffs, NJ: Prentice-Hall, 1968.

[21] S. Nakamura, "Applied Numerical Method in C," *Prentice-Hall int*. 1993.

[22] "A pratical Guide to Splines," *New York: Spring-Verlag*, 1987.